TAO, Vol. 11, No. 1, 337-348, March 2000

A Tomographic Study of Seasonal Variations of the Equatorial Anomaly in the Asian Sector

Wei-Hsiung Tsai[1, *], Lin-Fu Huang[1], Mei-Feng Chen[1] and Chao-Han. Liu[1]

(Manuscript received 28 January 2000, in final form 21 February 2000)

ABSTRACT

The Low-latitude Ionospheric Tomography Network (LITN) is used to investigate the seasonal behavior of the equatorial anomaly in the Asian Sector during a period of solar minimum. Seasonal variations of the location, the time of occurrence, and the height and the electron density of the maximum peak of the anomaly are studied. The starting time for the development of the anomaly and the lifetime of the whole phenomenon are also investigated. Extension of the work for possible 4D monitoring of the ionosphere using COSMIC data is discussed.

(Key words: Computerized Ionospheric Tomography (CIT), Equatorial anomaly region, Low-Latitude Ionospheric Tomography Network (LITN), Total Eletron Content (TEC))

1. INTRODUCTION

The concept of computerized ionospheric tomography(CIT) was first demonstrated by Austen et al. (1986; 1988). Since then the topic has attracted the interest of a large number of investigators to carry out further studies on both the theoretical and observational aspects of the problem (Raymund et al., 1990; Na and Lee, 1991; Yeh and Raymund, 1991; Kunitsyn and Tereshchenko, 1992; Fremouw et al., 1992; Pryse and Kersley, 1992; Raymund et al., 1994; Liu and Raymund, 1994; Huang et al., 1996; Fougere, 1995,1997; Kersley et al., 1997; Leitinger et al., 1984,1997; Antonio et al., 1998; Biswas and Na, 1998). In 1994, a low-latitude ionospheric tomography network along 120°E longitude was established to observe ionospheric structure in the equatorial anomaly region (Yeh et al., 1993). Initial results indicated that the network is capable of providing useful imagery of the ionosphere in this region (Huang et al., 1997, 1999). The network, the Low-Latitude Ionospheric Tomography Network (LITN), consists of a chain of six stations along the 120°E meridian: Shanghai (31.3°N, 121.5°E), Wenzhou (28.0°N, 120.6°E), Chung-Li (25.0°N, 120.6°E), Kaohsiung (22.5°N, 121.0°E), Baguio (16.4°N, 120.5°E) and Manila (14.6°N, 121.0°E) (Fig.1). Each station is equipped with a JMR 1 receiver and a data acquisition system to receive and record signals transmitted by the Naval

[1]Institute of Space Science, National Central University, Chung-Li, Taiwan, ROC

[*]*Corresponding author address*: Prof. Wei-Hsiung Tsai, Institute of Space Science, National Central University, Chung-Li, Taiwan, ROC; E-mail: Tomo@jupiter.ss.ncu.edu.tw

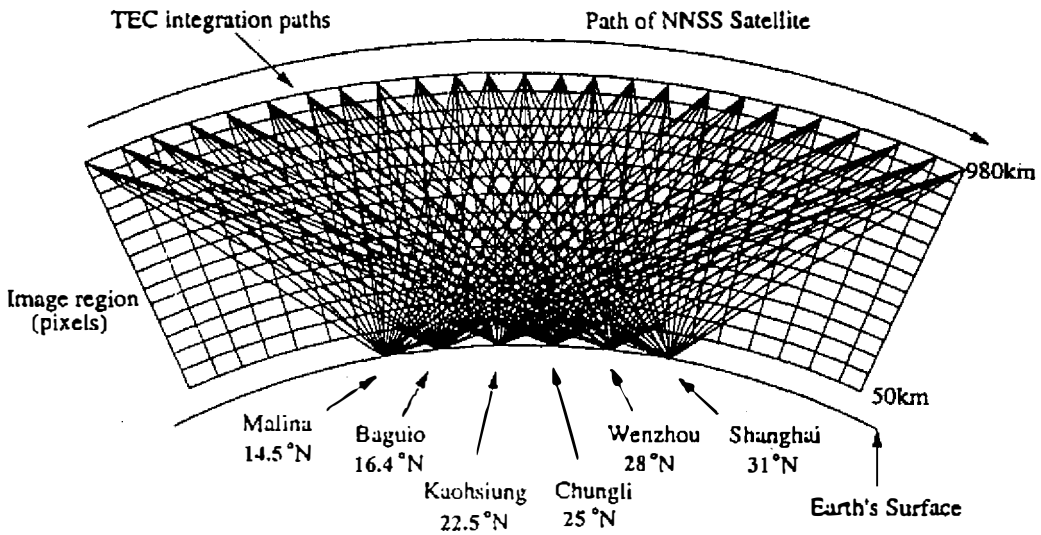

Fig.1. The tomography geometry for LITN shows ray paths from satellite to ground sation as a NNSS satellite transverses the image region over receiving station.

Navigation Satellite System (NNSS) from which total election content (TEC) can be derived. Figure 1 shows the geometry of the network and the radio rays emitted from the satellite and received at each station for one satellite path. The network was used successfully to image the ionosphere during the 24, October 1995 total eclipse occurred in this region (Huang et al., 1999). Between 1994 and 1997 when the NNSS signal was turned off, LITN was in routine operation. The data has been used to study a variety of ionospheric phenomena. In this paper, we shall concentrate on the seasonal variations of the ionosphere in the anomaly region. Cheng et al. (1992) and Huang and Cheng (1993) used the TEC data from a single station to investigate this problem. However, because of the sharp latitudinal variation of the ionosphere in this region, a multi-station tomographic technique such as LITN is more suitable for following the details of the variations. TEC data from LITN for the two-year period 1995-96 are used in the paper to reconstruct the ionosphere in the anomaly region in different seasons. From the reconstructed ionospheres, the behavior of the anomaly is investigated. In section 2, the computerized ionospheric tomography (CIT) technique is reviewed and some typical reconstructed images using LITN data are presented. The reconstructed ionospheres for different months are examined in section 3. These images are used to investigate the seasonal variations of the anomaly in section 4. In section 5, some conclusions are given and the possibility of 4D monitoring of the ionosphere using data from COSMIC is discussed.

2. COMPUTERIZED IONOSPHERE TOMOGRAPHY (CIT)

Figure1 shows a typical two-dimensional CIT geometry. Along any of the ray path connecting the satellite and the receiving station, the TEC is given by

$$C = \int_p N_e dS \,, \tag{1}$$

where C is the TEC, N_e is the electron density and p is the propagation path. For tomographic applications, Eq.(1) is approximated by the discrete sum

$$C_i = \sum_j^n a_{ij} x_j \,, \tag{2}$$

where C_i represents the TEC along the ith path, a_{ij} represents the length of the ith ray path in the jth pixel, and x_j is the election density in the jth pixel. Different algorithms have been developed to solve Eq.(2) to obtain the electron density distribution. Raymund et al. (1990) have shown the MART algorithm in detail, including the inversion procedure, initial guess and empirical model employed for the reconstruction in derail. For the LITN data reported in this paper the modified MART is used. Combining the estimated latitudinal distribution of the vertical TEC with ionosonde data, model inosphere, and Chapman ionospheric height distribution generates the initial guess required to start the iteration of the MART algorithm. This a priori information puts constraints in the reconstruction procedure on the peak electron density, the topside ionosphere distribution, and ionospheric heights. The details of the technique have been described by Huang et al. (1997, 1999). Figure 2 shows an example of the reconstruction using LITN geometry. We note that the technique is capable of reconstructing the major features of the ionosphere in the anomaly region.

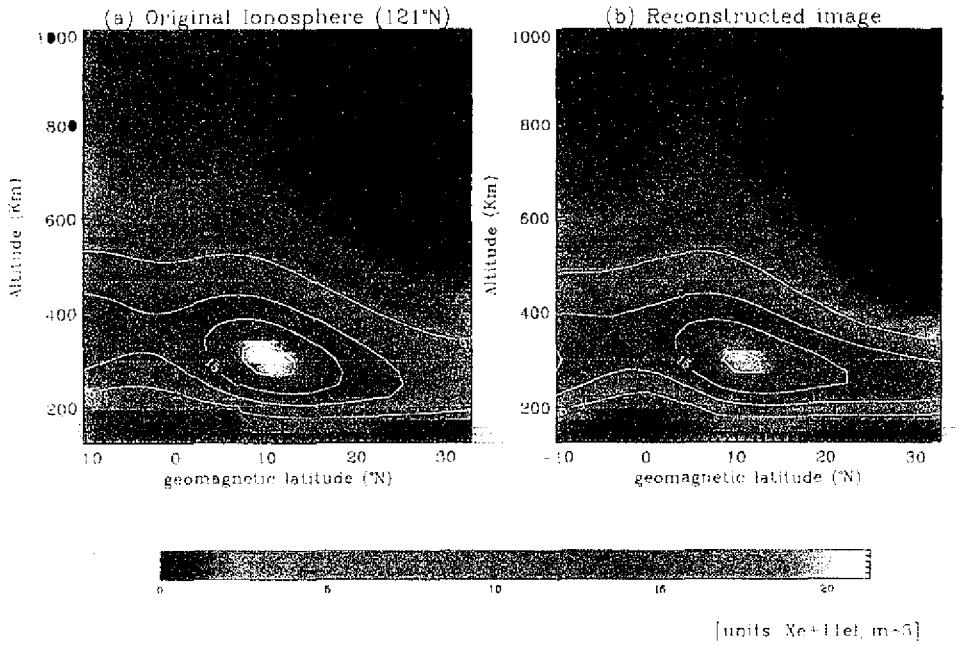

Fig. 2. (a) Ionospheric structure of IRI90 model used for the simulation. (b) Reconstructed image using the modified MART algorithm.

3. OBSERVATION AND RECONSTRUCTED N_e IMAGES

TEC data from NNSS at the LITN stations were analyzed for the two-year period 94-96. Reconstructions were carried out for cases where at least three stations recorded data of good quality. Figure 3 shows a typical example of vertical TEC distributions derived from LITN data. The passes at different times of the day provided us with a picture of the anomaly as it developed during the day on 8, March 1995. The anomaly started to develop before 09:26 LT. At that time, the peak was at 10°N. It began to move northward and grew in magnitude until it reached the highest peak value of 5.52×10^{17} electron/m^2 at 13:26 LT with the peak located at 24°N. After that, the peak moved south with decreasing magnitude until the anomaly disappeared altogether at 21:17 LT. Figure 4 shows examples of the tomographic images of the electron density reconstructed from the LITN data for several sample days at the time when the maximum peak of the anomaly occurred. From images like these, we can derive the position, the height and the electron density of the maximum peak of the anomaly. The information can then be used to study the seasonal variation of the anomaly when data from different months were used for reconstruction.

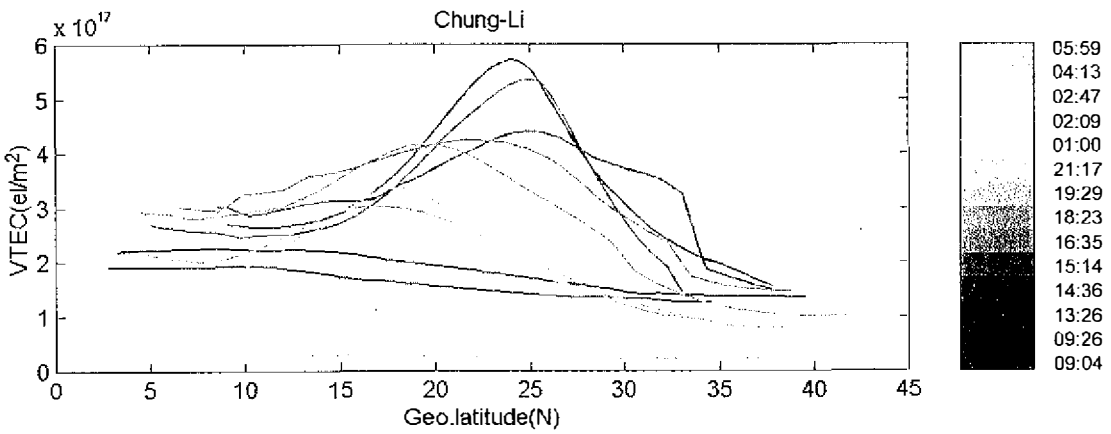

Fig.3. A typical example of vertical TEC distributions at different local time derived from LITN data.

4. SEASONAL VARIATION OF THE EQUATORIAL ANOMALLY IN THE ASIAN SECTOR

The data were taken from August 1994 to July 1996. During this period, the 12-month running average sunspot number ranged between 30 in 1994 to 10 in 1996. Therefore, it was a period when solar activity moved into its minimum. To investigate the seasonal behavior, we took five quiet days with the smallest k_p indices (<3) in each month and used them to represent the average behavior of the month.

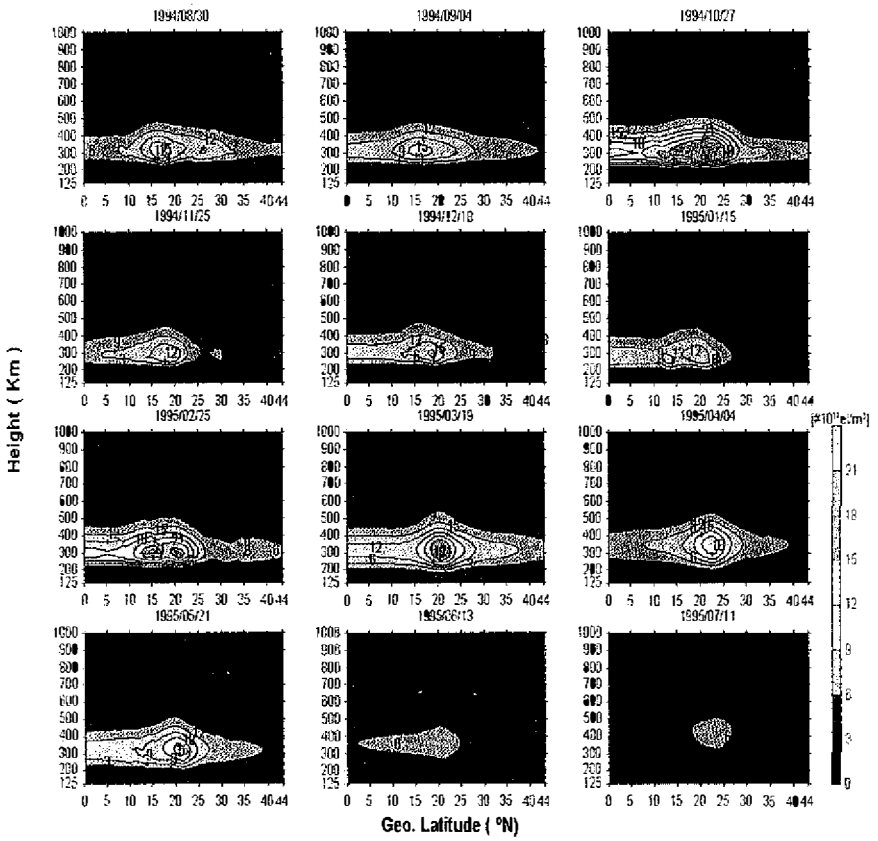

Fig.4. The tomographic images of the electron desity reconstructed from LITN data for several sample days at the time when the maximum peak of the anomaly occurred.

4.1 The Appearance and the Position of the Maximum Peak

The appearance of the anomaly is governed by the F-region dynamic processes, which are related to the motions and energetics of both the ionosphere and the thermosphere. It is expected that the position where the maximum peak electron density occurs and the time when the density grows to its peak value be closely related to these processes. Thus the behavior of the maximum peak may carry important information that can be used to study these dynamic processes. Our data provided a good opportunity to investigate the monthly behavior of the maximum peak. Figures 5a and 5b show the monthly distribution of the position of the maximum peak and its appearance time for the period from August 1994 to July 1996. The horizontal and vertical lines in Figs. 5a and 5b show the median values of latitude and the time of occurrence of the maximum crest in the five quiet days for each month. Figure 6a shows that for the two-year period studied, the peak appeared earlier during winter and summer as compared to the corresponding times during spring and autumn. The difference is even more pronounced during the solar minimum period 1995-96, as shown in Fig. 6b. There was also dis-

cernible asymmetry as the appearance time was pushed back further to around 18LT during autumnal equinox as compared to around 16LT during vernal equinox. A similar type of asymmetry was observed by Cheng(1992). We next consider the position of the peak shown in Figs. 7a and 7b. The peak moved to a higher latitude during spring and autumn. There was also an asymmetry as the peak moved further north during the vernal equinoctial month. It is also interesting to note the monthly variations of the magnitude of the TEC value shown in Fig. 8. Similar results and some possible mechanisms responsible for this asymmetry have been reported by Huang et al. (1989). We summarize the seasonal behavior of the maximum peak as follows: the maximum peak of the anomaly occurred later at local time at higher latitudes with higher TEC values during spring and autumn. There was an asymmetry in the behavior of the time and location of the peak between the autumn and vernal equinoxes. However, the no asymmetry seems for the magnitude of the TEC to exist.

4.2 Seasonal Variations of other Phases of the Anomaly

In addition to the maximum peak of the anomaly, other phases of the phenomenon as it develops during its whole life cycle are also of interest. Figures 9a and 9b show the monthly average TEC contours for the periods 1994-95 and 1995-96, respectively. We note that there

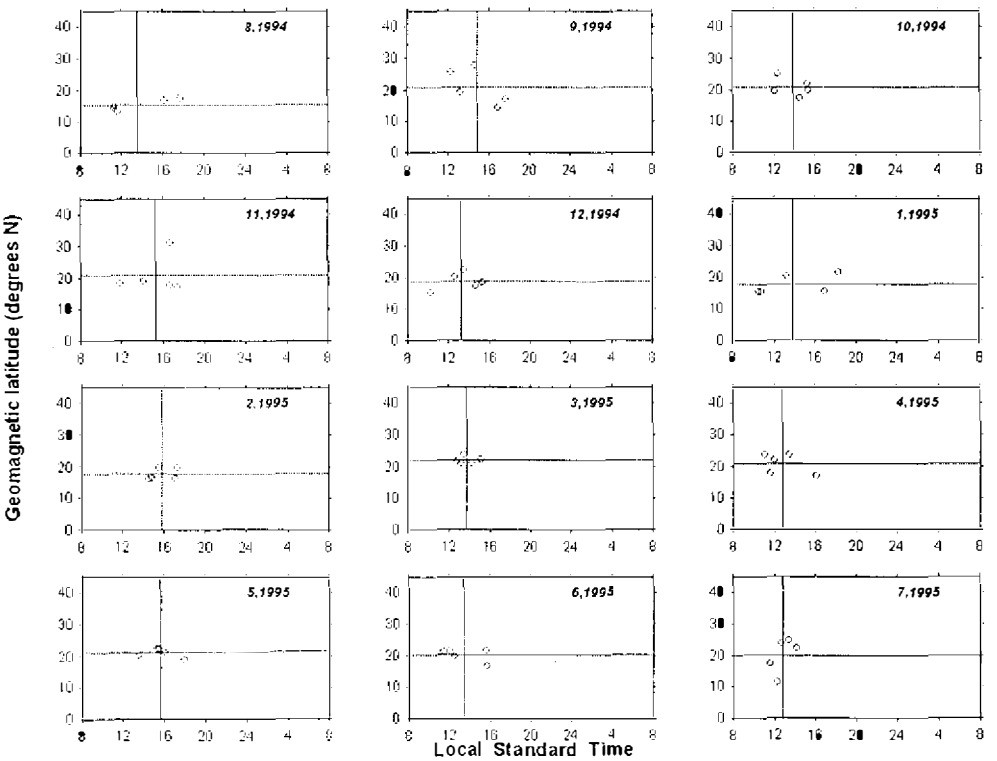

Fig. 5a The monthly distribution of the maximum peak appearance time and position for the 12 months period (94 - 95).

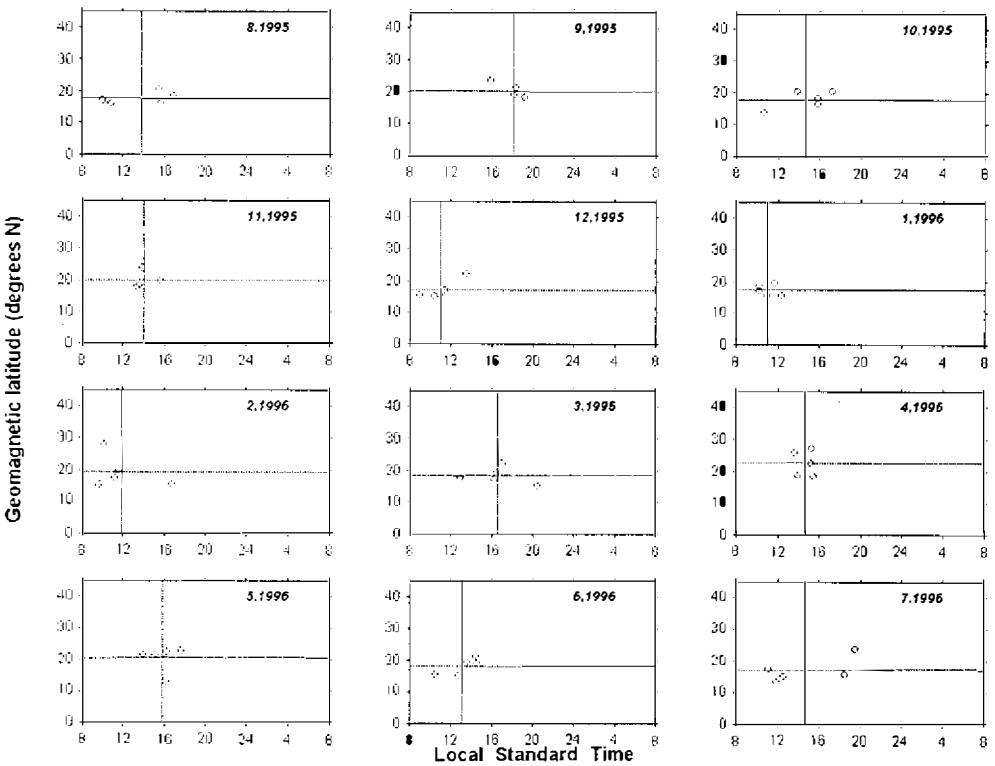

Fig. 5b. The monthly distribution of the maximum peak appearance time and position for the 12 months period (95 -96).

was hardly any seasonal variation of TEC between midnight and sunrise. The starting time for the development of the anomaly was around 08:00 LT and did not show any clear seasonal variation either. The anomaly disappeared between18:00 and 20:00LT in winter, at around 18:00LT in summer, and between 20:00 and 23:00LT in spring and autumn. Thus the lifetime of the anomaly is longer in spring and autumn, but shortest during summer. This may be caused mainly by the neutral wind blowing from the summer hemisphere to the winter hemisphere, which could inhibit the diffusion of plasma along field lines in the summer hemisphere (Rishbeth, 1972). It seems that seasonal anomaly of ionospheric electron density and seasonal variations of the electronic field strength have minor effects.

4.3 The Height and the Electron Density of the Maximum Peak

The reconstructed 2D images of the ionosphere for the time when the maximum peak occurred as shown in Fig. 4 can be used to study the vertical position of the maximum anomaly peak and the electron density at the peak. The results are shown in Fig. 10. The height of the maximum peak was found to be highest in summer, at around 410km, and lowest in winter, at around 300km. The electron density for the maximum peak was found to be largest during the equinox months and smallest during the month of the summer solstice. There seems to be a

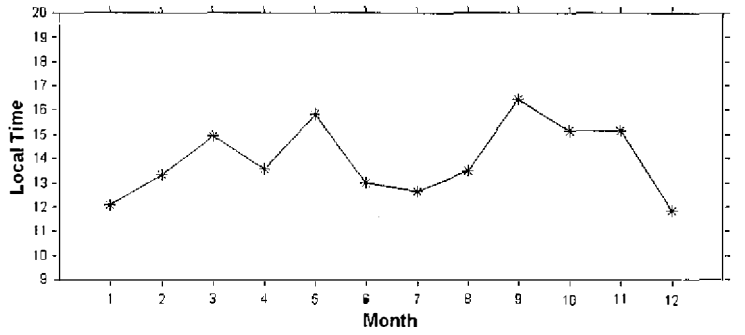

Fig. 6a. The two-year average monthly variation of the maximum peak with local time.

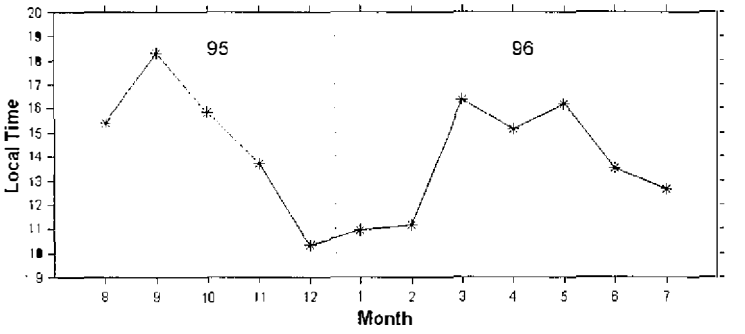

Fig. 6b. The monthly variation of the maximum peak with local time during the 95-96 period.

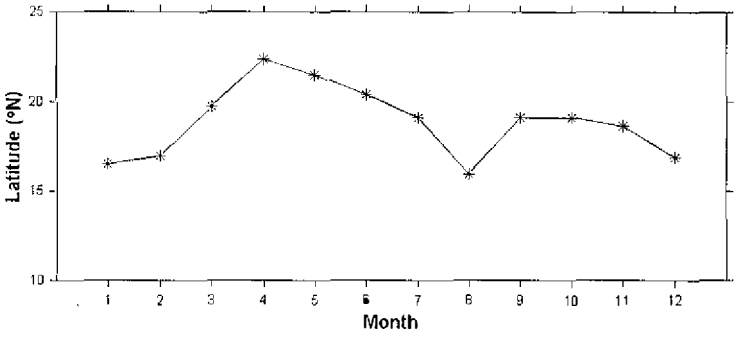

Fig. 7a. The two-year average monthly variation of the peak with latutude on LITN.

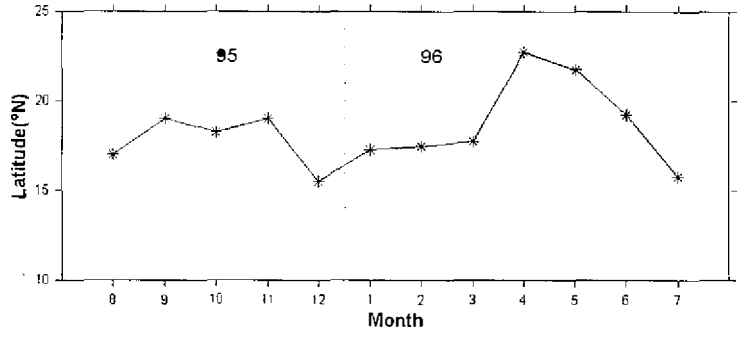

Fig. 7b. The monthly variation of the peak with latutude on LITN during the period 95-96.

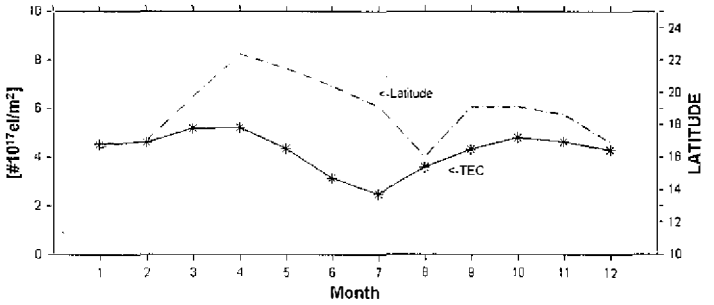

Fig. 8. The two-year monthly variations of the magnitude of the TEC value and location of the peak.

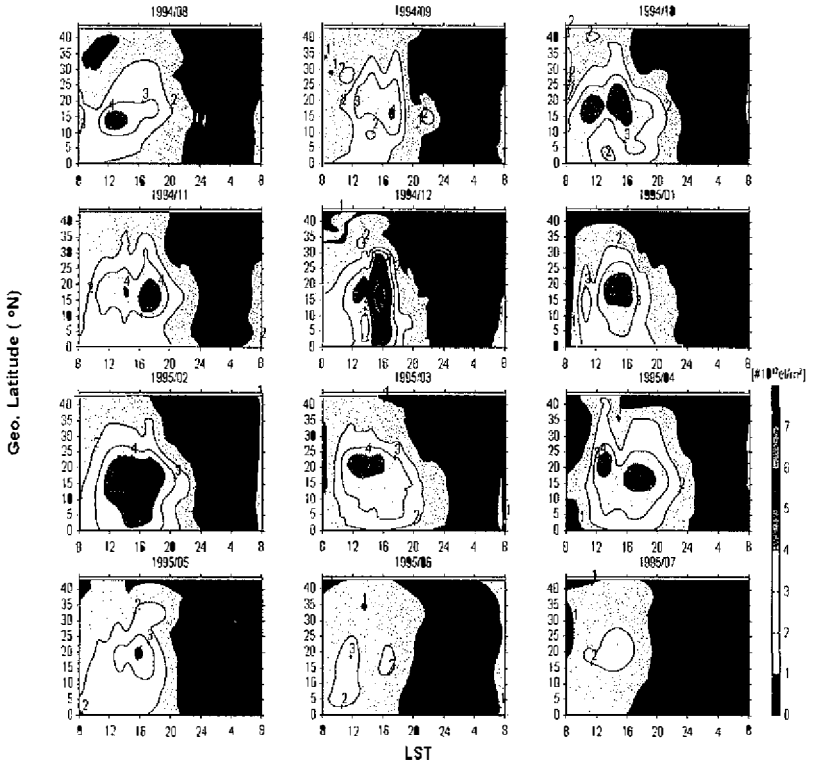

Fig. 9a. The monthly TEC contours for the one year period (94-95).

reverse correlation between the height and the electron density of the maximum peak.

5. DISCUSSIONS AND CONCLUSION

In this paper, we have used the data from LITN to study the seasonal variations of the equatorial anomaly in the Asian Sector. We have shown that the 2D tomographic images of the reconstructed ionosphere allow us to study seasonal variations in the time of occurrence, the height, the latitudinal location and the strength of the maximum peak, as well as the life-time of the anomaly. These results are very useful in the effort to model more accurately this

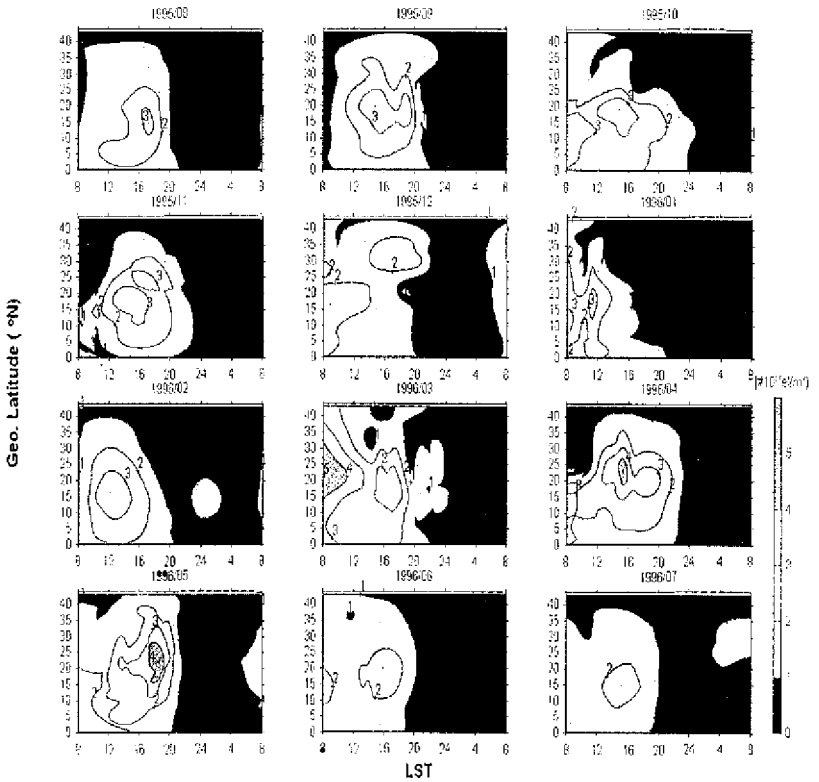

Fig. 9b. The monthly TEC contours for the one year period(95-96).

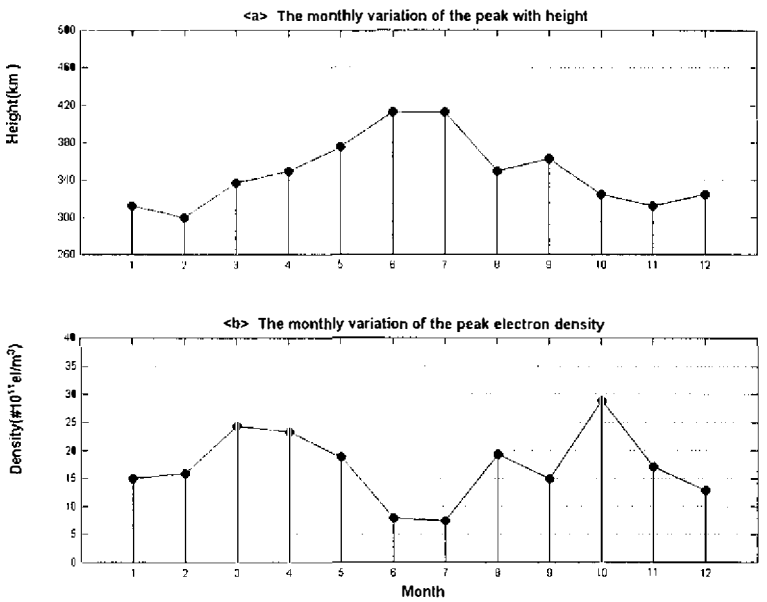

Fig. 10. (a) The monthly variation of the peak with height. (b) The monthly variation of the peak with electron density.

rather active region of the ionosphere, a task to be carried out in the near future. However, because of the limitation in the number of usable passes per day and the 2D nature in the reconstruction geometry, our results did not have very satisfactory temporal resolution and totally neglected the longitudinal variations. This situation may be significantly improved, however, with the launching of COSMIC. Data from the on-board GPS receivers and the network of ground-based stations for the Tri-Band Beacon experiment can be used for 4D ($\vec{r}$, t) tomographic reconstruction of the ionosphere. With these facilities in place, and the technique developed and experience gained in our current investigation, a real time monitoring of the equatorial anomaly and even the whole ionosphere, may become a reality.

Acknowledgments This work was supported by the National Science Council of the Republic of China under grant NSC 88-2111-M-008-014- AP9.

REFERENCES

Antonio, R., G. Ruffini, and A. Romeo, 1988: Analysis of Ionospheric Electron Density Distribution from GPD/MET Occultations. *IEEE antennas and Propagation Magazine.*, **36**, 383-394.

Austen, J. R., S. J. Franke, C. H. Liu, and K. C. Yeh, 1986: Applications of computerized tomography techniques to ionospheric research, International Beacon Satellite Symposium June, 9-14, Oulu Finland, Proceeding partl, 25-36.

Austen, J. R., S. J. Franke, and C. H. Liu, 1988: Ionosphere imaging using computerized tomography. *Radio Sci.*, **23**, 299-307.

Biswas, Chaitali, and Helen Na, 1998: Three-dimensional computerized ionospheric tomography using volumetric constraints. *Radio Sci.* **33**, 1793-1805.

Cheng, K., Y. N. Huang, and S. W. Chen, 1992: Ionospheric effects of the solar eclipse of September 23, 1987, around the equational anomaly crest region. *J. Geophys. Res.* **97**, 103-111.

Fougere, P. F., 1995: Ionospheric radio tomography using maximum entropy, 1, Theory and simulation studies. *Radio Sci.*, **30**, 429-444.

Fougere, P. F., 1997: Ionospheric radio tomography using maximum entropy, 2, Result of the Russian-American Tomography Experiment, including the large magnetic storm of November 3-4, 1993. *Radio Sci.*, **32**, 1623-1634.

Fremouw, E. J., J. A. Secan, and B. M. Howe, 1992: Application of stochastic inverse theory to ionospheric tomography. *Radio Sci.*, **27**, 721-732.

Huang, C. R., C. H. Liu, H. C. yeh, W. H. Tsai, C. J. Wang, K. C. Yeh, K. H. Lin, and H. L. Tsai, 1996: IRI model application in low latitude ionospheric tomography. *Adv. Space Res.*, **18 (6)**, 237-240.

Huang, C. R., C. H. Liu, H. C. Yeh, and W. H. Tsai, 1997: The low latitude ionospheric tomography network (LITN)—Initial Results. *J. Atmos. Terr. Phys.*, **59**, 1153-1167.

Huang, C. R., C. H. Liu , K. C. Yeh, W. H. Tasi, J. H. Liu, H. C. Yeh, 1999: A study of Tomographically Reconstructed Ionospheric Images during a Solar Eclipse. *J. Geophys. Res.* **104**, 79-94.

Huang, Y. N, K. Cheng, and S. W. Chen, 1989: On the Equatorial Anomaly of the Ionospheric Total Electron Content Near the Nothern Anomaly Crest Region. *J. Geophys. Res.* **94**, 13,515-13,525.

Huang, Y. N, K. Cheng, 1993: Ionospheric disturbances around East Asian region during the 20 October 1989 magnetic storm. *J. Atmos. Terr. Phys.*, **55**, 1009-1020.

Kersley, L., S. E. Pryse, I. K. Walker, J. A. T. Heaton, C. N. Mitchell, M. J. Williams, and C.A. Willson, 1997: Imaging of electron density troughs by tomographic techniques. *Radio Sci.*, **32**, 1607-1622.

Kunitsyn, V. E., and E. D. Tereshchenko, 1992: Radio tomography of the ionosphere. *IEEE antennas and Propagation Magazine*, **34**, 22-32.

Leitinger, R., G. Schmidt, and A. Tauriainen, 1984: An evaluation method combining the differential Doppler measurements from two station that enables the calculation of the electron content of the ionosphere. *J. Geophys.*, **41**, 201-213.

Leitinger, R., H. P. Ladreiter, and G. Kirchengast, 1997: Ionosphere tomography with data from satellite reception of Global Navigation Satellite System signals and ground reception of Navy Navigation Satellite System signals. *Radio Sci.*, **32**, 1657-1670.

Liu, C. H., and T. D. Raymund, 1994: Computerized ionospheric tomography and its applications, Proceeding of COSPAR colloquium on Low Latitude, Ionospheric Physics, edit by F. S. Kuo, 7, 285-293.

Na., H., and H. Lee, 1991: Orthogonal decomposition technique for ionospheric tomography. *Int. J. Imaging Sys. Technol.*, **3(4)**, 354-365.

Pryse, S. E., and L. Kersley., 1992: A preliminary test of ionospheric tomography. *J. Atmos. Terr. Phys.*, **54**, 1007-1012.

Raymund, T. D., J. R. Asten, S. J. Franke, C. H. Liu, J. A. Klobuchar, and J. Stalker, 1990: Application of computerized tomography to the investigation of ionospheric structures. *Radio Sci.*, **25**, 771-789.

Raymund, T. D., S. J. Franke, and K. C. Yeh, 1994: Ionospheric tomography: Its limitations and reconstruction method. *J. Atmos. Terr. Phys.*, **56**, 637-657.

Rishbeth, H., 1972: Thermospheric winds and the F-region -A Review. *J. Atmos. Terr. Phys.*, **34**, 1-47.

Yeh, K. C., and T. D. Raymund, 1991: Limitations of ionospheric imaging by tomography. *Radio Sci.*, **26**, 1361-1380.

Yeh, H. C., S.J. Franke, K. C. Yeh, C. H. Liu, T. D. Raymond, H. H. Chen, A. V. Izotov, J. Y. Liu, J. Wu, K. H. Lin, and S. W. Chen, 1993: Low-latitude Ionospheric Tomography Network along Taiwan meridian, Proceedings of COSPAR colloquium on Low Latitude Ionospheric Physics. In: F. S. Kuo (Ed.), 7, 295-303.